

Microstructure and velocity of field-driven solid-on-solid interfaces: Analytic approximations and numerical results

Per Arne Rikvold^{1,2,*} and M. Kolesik^{3,4,†}¹*Center for Materials Research and Technology, School of Computational Science and Information Technology and Department of Physics, Florida State University, Tallahassee, Florida 32306-4350*²*Department of Fundamental Sciences, Faculty of Integrated Human Studies, Kyoto University, Kyoto 606, Japan*³*Institute of Physics, Slovak Academy of Sciences, Bratislava, Slovak Republic*⁴*Optical Sciences Center, University of Arizona, Tucson, Arizona 85721*

(Received 9 April 2002; published 13 December 2002)

The local structure of a solid-on-solid interface in a two-dimensional kinetic Ising ferromagnet or attractive lattice-gas model with single-spin-flip Glauber dynamics, which is driven far from equilibrium by an applied field or chemical potential, is studied by an analytic mean-field, nonlinear-response theory [P. A. Rikvold and M. Kolesik, *J. Stat. Phys.* **100**, 377 (2000)], and by dynamic Monte Carlo simulations. The probability density of the height of an individual step in the surface is obtained, both analytically and by simulation. The width of the probability density is found to increase dramatically with the magnitude of the applied field, with close agreement between the theoretical predictions and the simulation results. Excellent agreement between theory and simulations is also found for the field dependence and anisotropy of the interface velocity. The joint distribution of nearest-neighbor step heights is obtained by simulation. It shows increasing correlations with increasing field, similar to the skewness observed in other examples of growing surfaces.

DOI: 10.1103/PhysRevE.66.066116

PACS number(s): 05.90.+m, 68.35.Ct, 75.60.Jk, 68.43.Jk

I. INTRODUCTION

The motion of surfaces and interfaces plays a central role in many scientific and technological disciplines. In particular, the dynamics of interfaces such as phase and grain boundaries in solid materials [1] and domain walls in magnets [2] and ferroelectrics heavily influence both dynamic and static material properties. Among interfaces characteristic of two-dimensional systems are steps on crystal surfaces [3], domain walls in thin magnetic and dielectric films [2], and boundaries between different types of vegetation such as savanna and rainforest [4].

An enormous amount of work in recent years has been devoted to the dynamics and structure of moving and growing interfaces [5,6]. However, despite the fact that many important interface properties, such as mobility and catalytic and chemical activity, are largely determined by the *microscopic* interface structure, most of this effort has been concentrated on large-scale scaling properties. Although the detailed atomistic mechanisms by which interfaces move are often not known, useful understanding can be obtained from stochastic models in which the motion occurs through random nucleation and migration of local topological features such as kinks and steps [1]. It is therefore important to gain better insight for different stochastic dynamics into how the driving force (such as an applied magnetic or electric field, a chemical-potential difference, or the amount of rainfall in the case of models of vegetation distribution) may alter the microscopic structure of the interface, thereby leading to a highly nonlinear velocity response.

In a previous paper [7], we introduced a dynamic mean-field approximation for the microstructure of an interface in a two-dimensional kinetic Ising ferromagnet with a single-spin-flip Glauber dynamic [8,9], driven by an applied field [10,11]. This model is directly applicable to many magnetic and ferroelectric systems and other cases where the interface dynamics are not inhibited by coupling to a conserved field [12,13]. Based on the resulting local interface structure, we obtained a nonlinear-response approximation for the steady-state propagation velocity, which was shown to be in good agreement with dynamic Monte Carlo (MC) simulations for a wide range of fields and temperatures. However, since the approximation was based on the Burton-Cabrera-Frank (BCF) unrestricted solid-on-solid (SOS) model [14], the overhangs and bubbles in the Ising interface were handled in an uncontrolled way. Here we therefore consider the performance of our approximation for the unrestricted SOS model, so that overhangs and bubbles are absent at all times by definition of the model. In particular, we obtain the surface velocity under the Glauber dynamic as a function of applied field and temperature, as well as its anisotropy for tilt angles between 0° and 45° .

In a recent paper [15], we showed that the microscopic interface structure, and thus the mobility, can depend dramatically on the details of the dynamics. The most significant difference is between dynamics in which the transition probabilities of the individual spins factorize into one part that depends only on the change in interaction energy due to the transition and one that depends only on the change in the field energy (soft dynamics [16]), and dynamics that cannot be factorized in this way (hard dynamics [16]). For soft dynamics, the interface structure for all values of the field remains the *same* as in equilibrium at zero field [15], so that a linear-response approximation yields an exact result for the

*Electronic address: rikvold@csit.fsu.edu

†Electronic address: kolesik@acms.arizona.edu

propagation velocity. In the present paper we concentrate on the standard Glauber dynamic [8,9], which belongs to the class of hard dynamics and thus leads to a more complicated and interesting behavior.

Both the driven Ising and SOS surfaces belong to the Kardar-Parisi-Zhang (KPZ) dynamic universality class [5,17], in which the macroscopic, stationary distribution for flat, moving interfaces is Gaussian, corresponding to a random walk with independent increments. Nevertheless, the step heights in several discrete models in this class are correlated at *short* distances [18–20]. In the mean-field approximation developed here, these short-range correlations are ignored. The resulting discrepancies, which are minor, will be elucidated by comparison with MC simulations.

The remainder of this paper is organized as follows. In Sec. II we introduce the SOS interface model and derive a linear-response approximation for its velocity in a nonzero external field. In Sec. III we develop a mean-field approximation for the time evolution of the single-step probability density function (PDF), as well as for its stationary form. The latter enables us to extend the approximation for the interface structure and velocity to a nonlinear-response level. The analytical approximations are compared with dynamic MC simulations in Sec. IV. In Sec. IV A we numerically solve the mean-field equation of motion for the single-step PDF and compare the resulting values of the time-dependent average interface step height with MC simulations. In Sec. IV B we compare the simulated stationary single-step PDFs with the theoretical predictions. In Sec. IV C we compare the simulated stationary interface velocity with the theoretical predictions for various values of applied field, temperature, and interface tilt angle. In Sec. IV D we compare simulations and analytical predictions for the detailed stationary interface structure, including the asymmetry of the simulated interface at nonzero fields. A summary and conclusion are found in Sec. V.

II. MODEL AND DYNAMICS

The original BCF SOS model considers an interface in a lattice gas or $S=1/2$ Ising system on a square lattice of unit lattice constant as a single-valued integer function $h(x)$ of the x coordinate, with steps $\delta(x)=h(x+1/2)-h(x-1/2)$ at integer values of x . A typical SOS interface configuration is shown in Fig. 1. In this paper, like in Refs. [7,15], we use the highly symmetric Ising language, in which the two possible states of the site (x,y) are denoted by the two “spin” values $s_{x,y}=\pm 1$. (In order that the step positions and the interface heights be integer as stated above, we place the spins at odd half-integer values of x and y , i.e., at the centers of the unit cells separated by dotted lines in Fig. 1.) The configuration energy is given by the nearest-neighbor Ising Hamiltonian with anisotropic, ferromagnetic interactions J_x and J_y in the x and y direction, respectively:

$$\mathcal{H} = - \sum_{x,y} s_{x,y} (J_x s_{x+1,y} + J_y s_{x,y+1} + H), \quad (1)$$

where $\sum_{x,y}$ runs over all sites. The quantity H is the applied “field,” and the interface is introduced by fixing $s_{x,y}=+1$

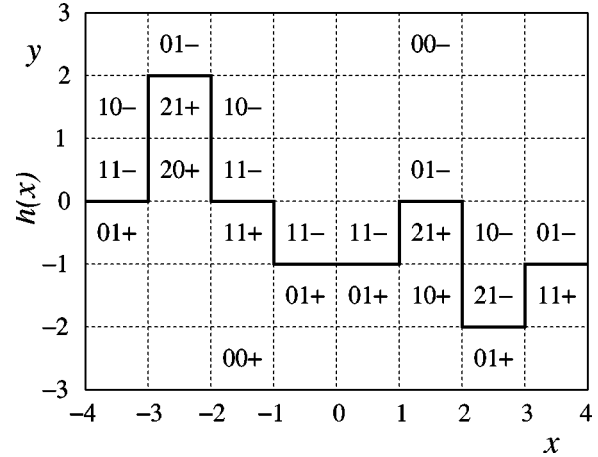


FIG. 1. A short segment of an SOS interface $y=h(x)$ between a positively magnetized phase (or “solid” phase in the lattice-gas picture) below and a negative (or “fluid”) phase above. The step heights are $\delta(x)=h(x+1/2)-h(x-1/2)$. Interface sites representative of the different SOS spin classes (see Table I and Table II) are marked with the notation jks explained in the text. Sites in the uniform bulk phases are $00-$ and $00+$. This interface was generated with a symmetric step-height distribution, corresponding to $\phi=0$, but it would be impossible to estimate ϕ accurately from the short segment shown here. After Ref. [7].

and -1 for large negative and positive y , respectively. Without loss of generality we take $H \geq 0$, such that the interface on average moves in the positive y direction. This Ising model is equivalent to a lattice-gas model with local occupation variables $c_{x,y} \in \{0,1\}$ [21,22]. Specifically, we identify $s=+1$ with $c=1$ (occupied or “solid”) and $s=-1$ with $c=0$ (empty or “fluid”). The applied field is related to the lattice-gas chemical potential μ as $H=(\mu-\mu_0)/2$, where $\mu_0=-4(J_x+J_y)$ is the coexistence value of μ . In this paper we use Ising or lattice-gas language interchangeably as we feel it makes a particular aspect of the discussion clearer.

A single-spin-flip (nonconservative) dynamic which satisfies detailed balance, such as the Metropolis or Glauber algorithms [8,9], ensures the approach to equilibrium, which in this case is a uniformly positive phase with the interface pushed off to positive infinity. Such algorithms are defined by a single-spin transition probability, $W(s_{x,y} \rightarrow -s_{x,y}) = W(\beta\Delta E, \beta U)$. Here β is the inverse of the temperature T (Boltzmann’s constant is taken as unity), ΔE is the energy change corresponding to a successful spin flip, and the optional parameter U is an energy barrier between the two states that enters into Arrhenius-type stochastic dynamics [23] and other dynamics that include a transition state [24]. The detailed-balance condition (valid for transitions between allowed states) is expressed as $W(\beta\Delta E, \beta U)/W(-\beta\Delta E, \beta U) = e^{-\beta\Delta E}$, where the right-hand side is independent of U . (In the case of soft dynamics, the detailed-balance condition is satisfied independently for the two parts of W .) In order to preserve the SOS configuration at all times, flips are allowed only at sites which have exactly one broken bond in the y direction.

With the Ising Hamiltonian there are only a finite number of different values of ΔE , and the spins can therefore be

TABLE I. The spin classes in the anisotropic square-lattice SOS model. The first column contains the class labels, jks . The second column contains the total field and interaction energy for a spin in each class, $E(jks)$, relative to the energy of the state with all spins parallel and $H=0$, $E_0 = -2(J_x + J_y)$. The third column contains the change in the total system energy resulting from reversal of a spin from s to $-s$, $\Delta E(jks)$. In both $E(jks) - E_0$ and $\Delta E(jks)$, the upper sign corresponds to $s = -1$, and the lower sign to $s = +1$.

Class, jks	$E(jks) - E_0$	$\Delta E(jks)$
01s ^a	$\pm H + 2J_y$	$\mp 2H + 4J_x$
11s ^a	$\pm H + 2(J_x + J_y)$	$\mp 2H$
21s ^a	$\pm H + 2(2J_x + J_y)$	$\mp 2H - 4J_x$
10s ^b	$\pm H + 2J_x$	$\mp 2H + 4J_y$
20s ^b	$\pm H + 4J_x$	$\mp 2H - 4(J_x - J_y)$

^aThe classes having nonzero populations in the SOS model and in which flipping a spin preserves the SOS configuration.

^bThe classes having nonzero populations in the SOS model and in which flipping a spin would produce an overhang or a bubble and is therefore forbidden.

divided into classes [11,25,26], labeled by the spin value s and the number of broken bonds between the spin and its nearest neighbors in the x and y direction, j and k , respectively. The ten spin classes consistent with the SOS model are denoted jks with $j \in \{0,1,2\}$ and $k \in \{0,1\}$. They are shown in Fig. 1 and listed in Table I and Table II.

TABLE II. The mean populations for the spin classes of the SOS interface, with the corresponding contributions to the interface velocity under the hard Glauber dynamic. The first column contains the class labels, jks . The second column contains the mean spin-class populations for general tilt angle ϕ , with $\cosh \gamma(\phi)$ from Eq. (5). The third and fourth columns contain the spin-class populations for $\phi = 0$ [using $\gamma(0) = 0$] and $\phi = 45^\circ$ (using Eq. (7) for $\exp[\gamma(45^\circ)]$), respectively. Using $X = e^{-2\beta J_x}$ in these expressions yields the linear-response result in which the spin-class populations are evaluated for $H = 0$. Using $X = X(T, H)$ from Eq. (17) with the transition probabilities of the particular dynamic used [here, Glauber, so that $X(T, H)$ is explicitly given by Eq. (18)], one gets the nonlinear-response approximation. The fifth column contains the contributions to the mean interface velocity in the y direction from spins in classes $jk-$ and $jk+$, Eq. (9), using the SOS-preserving hard Glauber dynamic.

Class, jks	$\langle n(jks) \rangle$, general ϕ	$\langle n(jks) \rangle$, $\phi = 0$	$\langle n(jks) \rangle$, $\phi = 45^\circ$	$\langle v_y(jk) \rangle$
01s	$\frac{1 - 2X \cosh \gamma(\phi) + X^2}{(1 - X^2)^2}$	$\frac{1}{(1 + X)^2}$	$\frac{1}{2(1 + X^2)}$	$\frac{\tanh(\beta H)}{1 + \left[\frac{\sinh(2\beta J_x)}{\cosh(\beta H)} \right]^2}$
11s	$\frac{2X[(1 + X^2)\cosh \gamma(\phi) - 2X]}{(1 - X^2)^2}$	$\frac{2X}{(1 + X)^2}$	$\frac{1}{2}$	$\tanh(\beta H)$
21s	$\frac{X^2[1 - 2X \cosh \gamma(\phi) + X^2]}{(1 - X^2)^2}$	$\frac{X^2}{(1 + X)^2}$	$\frac{X^2}{2(1 + X^2)}$	$\frac{\tanh(\beta H)}{1 + \left[\frac{\sinh(2\beta J_x)}{\cosh(\beta H)} \right]^2}$
10s	$\frac{2X^2}{1 - X^2} \left\{ \frac{2 \cosh^2 \gamma(\phi) - 1 - 2X \cosh \gamma(\phi) + X^2}{1 - 2X \cosh \gamma(\phi) + X^2} - \frac{X^2[1 - 2X \cosh \gamma(\phi) + X^2]}{(1 - X^2)^2} \right\}$	$\frac{2X^2(1 + 2X)}{(1 - X^2)(1 + X)^2}$	$\frac{1 + 2X^2 + 3X^4}{2(1 - X^4)}$	0
20s	$\frac{X^4[1 - 2X \cosh \gamma(\phi) + X^2]}{(1 - X^2)^3}$	$\frac{X^4}{(1 - X^2)(1 + X)^2}$	$\frac{X^4}{2(1 - X^4)}$	0

In this paper, as in Ref. [7], we use the standard discrete-time (hard) Glauber dynamic with the transition probability [8,9]

$$W_G(s_{x,y} \rightarrow -s_{x,y}) = [1 + e^{\beta \Delta E}]^{-1} \quad (2)$$

for all transitions that are allowed by the SOS constraint. Time is measured in MC steps per spin (MCSS).

In the BCF SOS model the heights of the individual steps are assumed to be statistically independent and identically distributed. The step-height PDF is given by the interaction energy corresponding to the $|\delta(x)|$ broken J_x -bonds between spins in the columns centered at $(x - 1/2)$ and $(x + 1/2)$ as

$$p[\delta(x)] = Z(\phi)^{-1} X^{|\delta(x)|} e^{\gamma(\phi)\delta(x)}. \quad (3)$$

The Boltzmann factor $X = e^{-2\beta J_x}$ determines the width of the PDF, and $\gamma(\phi)$ is a Lagrange multiplier which maintains the mean step height at an x -independent value, $\langle \delta(x) \rangle = \tan \phi$, where ϕ is the overall angle between the interface and the x axis. The partition function is

$$Z(\phi) = \sum_{\delta=-\infty}^{+\infty} X^{|\delta|} e^{\gamma(\phi)\delta} = \frac{1 - X^2}{1 - 2X \cosh \gamma(\phi) + X^2}, \quad (4)$$

with $\gamma(\phi)$ given by

$$e^{\gamma(\phi)} = \frac{(1 + X^2)\tan \phi + [(1 - X^2)^2 \tan^2 \phi + 4X^2]^{1/2}}{2X(1 + \tan \phi)} \quad (5)$$

(see details in Ref. [7]). Simple results are obtained for $\phi = 0$, which yields $\gamma(0) = 0$ and

$$Z(0) = (1 + X)/(1 - X), \quad (6)$$

and for $\phi = 45^\circ$, which yields

$$e^{\gamma(45^\circ)} = (1 + X^2)/2X \quad (7)$$

and

$$Z(45^\circ) = 2(1 + X^2)/(1 - X^2). \quad (8)$$

The mean spin-class populations $\langle n(jks) \rangle$ are all obtained from the product of the independent PDFs for $\delta(x)$ and $\delta(x+1)$. Symmetry of $p[\delta(x)]$ under the transformation $(x, \phi, \delta) \rightarrow (-x, -\phi, -\delta)$ ensures that $\langle n(jk-) \rangle = \langle n(jk+) \rangle$ for all j and k . Numerical results illustrating the breakdown of this up/down symmetry for large $|H|$ are discussed in Sec. IV D. As discussed in Ref. [7], calculation of the individual class populations is straightforward but somewhat tedious, especially for nonzero ϕ . The final results are summarized in Table II.

Whenever a spin flips from -1 to $+1$, the corresponding column of the interface advances by one lattice constant in the y direction. Conversely, the column recedes by one lattice constant when a spin flips from $+1$ to -1 . The corresponding energy changes are given in the third column in Table I. Since the spin-class populations on both sides of the interface are equal in this approximation, the contribution to the mean velocity in the y direction from sites in the classes $jk-$ and $jk+$ becomes

$$\langle v_y(jk) \rangle = W(\beta\Delta E(jk-), \beta U) - W(\beta\Delta E(jk+), \beta U). \quad (9)$$

The results corresponding to the hard Glauber transition probabilities used here, Eq. (2), are listed in the last column of Table II. The mean propagation velocity perpendicular to the interface becomes

$$\langle v_\perp(T, H, \phi) \rangle = \cos \phi \sum_{j,k} \langle n(jks) \rangle \langle v_y(jk) \rangle, \quad (10)$$

where the sum runs over the classes included in the tables. While the general result is cumbersome if written out in detail, the special cases of $\phi = 0$ and $\phi = 45^\circ$ lead to compact formulas

$$\langle v_\perp(T, H, 0) \rangle = \frac{\tanh(\beta H)}{(1 + X)^2} \left\{ 2X + \frac{1 + X^2}{1 + \left[\frac{\sinh(2\beta J_x)}{\cosh(\beta H)} \right]^2} \right\} \quad (11)$$

and

$$\langle v_\perp(T, H, 45^\circ) \rangle = \frac{\tanh(\beta H)}{2\sqrt{2}} \left\{ 1 + \frac{1}{1 + \left[\frac{\sinh(2\beta J_x)}{\cosh(\beta H)} \right]^2} \right\}, \quad (12)$$

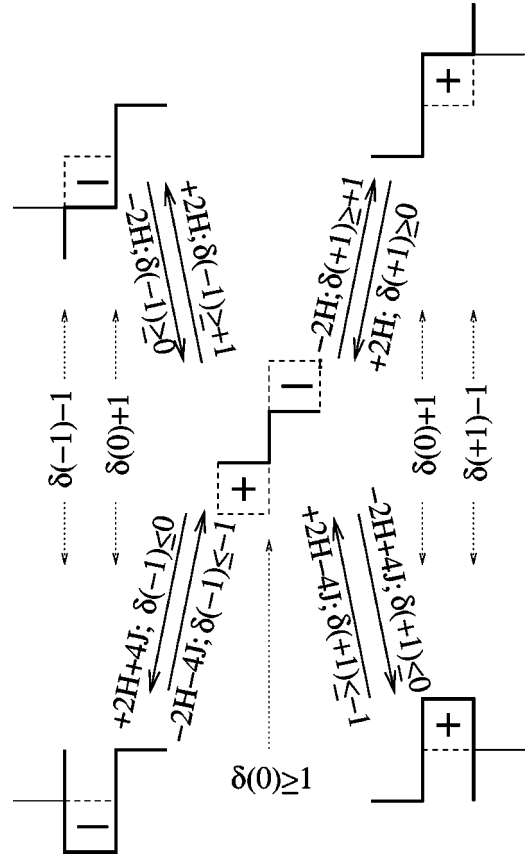


FIG. 2. Figure for calculating the single-step transition rates in Eq. (14). Interface configurations are shown by bold line segments. Spins above (in front of) the interface equal -1 , and spins below (behind) the interface equal $+1$. At the center is shown a step $\delta(0) \geq 1$ [here shown as $\delta(0) = +1$]. A transition to $\delta(0) + 1$ can be effected by flipping either of the two spins in the dashed boxes. The resulting configurations, which depend on the heights of the neighboring steps, are shown to the right and left in the figure. The corresponding energy changes and conditions on the neighboring step heights are given next to the arrows. The arrows pointing outward from the center of the figure correspond to the transition described above, while the arrows pointing toward the center correspond to the reverse transition, $\delta(0) + 1 \rightarrow \delta(0)$. In this figure, J stands for J_x . After Ref. [7].

respectively. It was shown in Ref. [7] that Eq. (10) reduces to the results for the single-step [10,11,27,28] and the polynuclear growth [10,29,30] models at low temperatures for strong and weak fields, respectively.

III. NONLINEAR RESPONSE

With $X = e^{-2\beta J_x}$, the results in Table II correspond to a linear-response approximation. In Ref. [7] we developed a mean-field approximation leading to a field-dependent $X(T, H)$, based on a detailed-balance argument for the stationary state. Here we show that this detailed-balance relation follows naturally from a dynamic mean-field approximation for the equation of motion for the single-step PDF during the approach to the stationary state.

We denote the total transition probability for the height of

the single step at x to change from $\delta(x)$ to $\delta(x) \pm 1$ as $\mathcal{W}[\delta(x) \rightarrow \delta(x) \pm 1]$. In terms of these transition probabilities, the equation of motion for the single-step PDF, $p[\delta(x), t]$ becomes

$$\begin{aligned} \frac{dp[\delta(x), t]}{dt} = & -p[\delta(x), t] \{ \mathcal{W}[\delta(x) \rightarrow \delta(x) - 1] \\ & + \mathcal{W}[\delta(x) \rightarrow \delta(x) + 1] \} \\ & + p[\delta(x) + 1] \mathcal{W}[\delta(x) + 1 \rightarrow \delta(x)] \\ & + p[\delta(x) - 1] \mathcal{W}[\delta(x) - 1 \rightarrow \delta(x)], \end{aligned} \quad (13)$$

where the coupling to the joint multistep probability density is hidden in the single-step transition rates \mathcal{W} (not to be confused with the single-site transition rates W).

To obtain an approximation for $\mathcal{W}[\delta \rightarrow \delta \pm 1]$, we employ the same mean-field assumption of independent steps as in equilibrium. For $\delta(x) \geq 1$ to increase to $\delta(x) + 1$, either the spin in front of the interface at $x + 1/2$ can flip from -1 to $+1$, or the spin behind the interface at $x - 1/2$ can flip from $+1$ to -1 . In each of these cases, ΔE can have two different values, depending on the value of $\delta(x + 1)$ and $\delta(x - 1)$, respectively. The same argument holds also for the reverse transition, $\delta(x) + 1 \rightarrow \delta(x)$. The energy changes and corresponding conditions on $\delta(x + 1)$ and $\delta(x - 1)$, which are shown in Fig. 2, yield

$$\begin{aligned} \mathcal{W}[\delta \rightarrow \delta \pm 1, t] = & \frac{1}{2} \{ [W(-2H) + W(+2H)] \Pi_{\pm}(t) \\ & + [W(-2H + 4J_x) + W(+2H + 4J_x)] \\ & \times [1 - \Pi_{\pm}(t)] \}, \end{aligned}$$

which is independent of $\gamma(\phi)$. This solution is the same as the one obtained in Ref. [7], but the derivation given in that paper did not explicitly show that all dependence on $\gamma(\phi)$ cancels out. The fact that $X(T, H)$ does not depend on $\gamma(\phi)$ is fortunate, since it enables both quantities to be calculated analytically. If this were not the case, they would have had to be determined by simultaneous numerical solution of Eqs. (17) and (5).

Equation (17) shows that $X(T, H)$ depends on the specific dynamic, except for $H=0$, where it reduces to its equilibrium value, $X(T, 0) = e^{-2\beta J_x}$. A situation in which the H dependence in Eq. (17) cancels out, is that of the soft dynamics discussed in Sec. I. (The barrier energy U can be contained in one or the other of the factors.) In Ref. [15] we demonstrated that a soft dynamic yields an SOS interface that is identical to the equilibrium SOS interface at $H=0$ and the same temperature, regardless of the value of H . Neither the

$$\begin{aligned} \mathcal{W}[\delta \pm 1 \rightarrow \delta, t] = & \frac{1}{2} \{ [W(-2H) + W(+2H)] [1 - \Pi_{\mp}(t)] \\ & + [W(-2H - 4J_x) + W(+2H - 4J_x)] \\ & \times \Pi_{\mp}(t) \}, \end{aligned} \quad (14)$$

where the upper signs refer to $\delta \geq +1$ and the lower signs to $\delta \leq -1$, $\Pi_{+}(t) = \sum_{\delta=+1}^{+\infty} p[\delta, t]$, and $\Pi_{-}(t) = \sum_{\delta=-1}^{-\infty} p[\delta, t]$. For simplicity, we here write the single-site transition rates $W(\beta \Delta E, \beta U)$ as $W(\Delta E)$.

In the stationary limit, Eqs. (13) and (3) lead to the detailed-balance condition

$$X(T, H) e^{\pm \gamma(\phi)} \equiv \frac{p[\delta \pm 1]}{p[\delta]} = \frac{\mathcal{W}[\delta \rightarrow \delta \pm 1]}{\mathcal{W}[\delta \pm 1 \rightarrow \delta]}, \quad (15)$$

where the upper and lower signs have the same interpretation as in Eq. (14). Using Eqs. (3) and (4), we get the stationary values for Π_{+} and Π_{-} ,

$$\begin{aligned} \Pi_{+} &= \frac{X e^{\gamma(\phi)} (1 - X e^{-\gamma(\phi)})}{1 - X^2}, \\ \Pi_{-} &= \frac{X e^{-\gamma(\phi)} (1 - X e^{\gamma(\phi)})}{1 - X^2}, \end{aligned} \quad (16)$$

which, when inserted together with Eq. (14) in Eq. (15), yield a self-consistency equation for X . The self-consistency equation reduces to a linear equation for X^2 , and with the help of the detailed-balance condition for the single-site transition rates W , the solution takes the form

$$X(T, H) = e^{-2\beta J_x} \left\{ \frac{e^{-2\beta H} W(-2H - 4J_x) + e^{2\beta H} W(+2H - 4J_x)}{W(-2H - 4J_x) + W(+2H - 4J_x)} \right\}^{1/2}, \quad (17)$$

Glauber dynamic used here, nor the equally common Metropolis dynamic with transition probability $W_M(s_{x,y} \rightarrow -s_{x,y}) = \min[1, e^{-\beta \Delta E}]$ [8,9], satisfies this factorization condition. Such hard dynamics lead to a nontrivial field dependence in X . Inserting the Glauber dynamic defined by Eq. (2) into Eq. (17), we explicitly get

$$X_G(T, H) = e^{-2\beta J_x} \left\{ \frac{e^{2\beta J_x} \cosh(2\beta H) + e^{-2\beta J_x}}{e^{-2\beta J_x} \cosh(2\beta H) + e^{2\beta J_x}} \right\}^{1/2}. \quad (18)$$

All the results for the spin-class populations of the zero-field equilibrium interface, which are listed in Table II, can now be applied to obtain a nonlinear-response approximation for the steady-state propagation velocity of flat, driven interfaces with hard dynamics. This simply requires replacing the zero-field $X = e^{-2\beta J_x}$ used in the linear-response approxima-

tion by the field-dependent $X(T, H)$, obtained from Eq. (17) using the transition probabilities corresponding to the particular dynamic used. For soft dynamics the linear-response result with $X = e^{-2\beta J_x}$ is exact.

A physical reason for the marked difference between hard and soft dynamics is best seen by comparing concrete examples of dynamics in the two classes, such as the hard Glauber dynamic used here, Eq. (2), and the soft Glauber dynamic used in Ref. [15],

$$W_{SG}(s_{x,y} \rightarrow -s_{x,y}) = \frac{e^{-\beta\Delta E_H}}{1 + e^{-\beta\Delta E_H}} \frac{e^{-\beta\Delta E_J}}{1 + e^{-\beta\Delta E_J}}, \quad (19)$$

in the case of a very strong field. In the hard case, the effect of the field completely dominates the transition rates, such that the rate is near unity for transitions that bring a spin parallel to the applied field, and near zero for transitions in the opposite direction, *irrespective of the change in interaction energy*. In the soft case, the probability of bringing a spin antiparallel to the field is also near zero, but the probabilities of different transitions bringing a spin parallel to the field differ according to the corresponding change in the interaction energy, as given by the second factor in Eq. (19).

In the following section we show that the nonlinear-response approximation developed in this section gives very good agreement with MC simulations of driven, flat SOS interfaces evolving under the hard Glauber dynamic for a wide range of fields and temperatures.

IV. COMPARISON WITH MONTE CARLO SIMULATIONS

We have compared the analytical estimates of step-height distributions, propagation velocities, and spin-class populations developed above with MC simulations of the same model for $J_x = J_y = J$. The details of our particular implementation of the discrete-time n -fold way rejection-free MC algorithm [25] are the same as described in Ref. [7], except that only transitions from the classes with one broken y bond ($k=1$) are allowed. By keeping only the interface sites in memory, the algorithm is not subject to any size restriction in the y direction, and simulations can be carried out for arbitrarily long times.

The numerical results presented here are based on MC simulations at the two temperatures, $T=0.2T_c$ and $0.6T_c$ [$T_c = -2J/\ln(\sqrt{2}-1) \approx 2.269J$ is the critical temperature for the isotropic, square-lattice Ising model [31]], with $L_x = 10\,000$ and fixed ϕ between 0 and 45° . In order to ensure stationarity we ran the simulation for 5 000 n -fold way updates per updatable spin (UPS) before taking any measurements (100 000 UPS for some of the strongest fields and largest values of ϕ at $T=0.2T_c$). Exploratory simulations with both larger and smaller L_x (up to 100 000) and “warm-up” times (see Sec. IV A) showed that the values used in the production runs were sufficient to ensure a stationary interface. Stationary class populations and interface velocities were averaged over 50 000 UPS. In the stationary limit 1 UPS corresponds to between 2 MCSS for strong fields at both temperatures, and about 75 MCSS for $H=0$ at $T=0.2T_c$. Adequate statistics for one- and two-step PDFs was

ensured by the large L_x , ten times the value used in Refs. [7,32].

A. Approach to the stationary state

In order to both check the applicability of the mean-field approximation at early times, and decide the approximate time needed to reach the stationary state, we first studied the transient behavior of the average step height $\langle |\delta| \rangle$ for $\phi = 0$ at $T=0.2J$ and $0.6J$.

In the dynamic MC simulation $\langle |\delta| \rangle$ was measured during a “time window” which was opened after a specified number of UPS, corresponding to a given approximate average evolution time t in MCSS. To obtain an optimum balance between time resolution and accuracy, the width of the window was varied from approximately one MCSS at early times, to about ten MCSS at late times, and five independent runs were performed for each value of t . Standard errors for t and $\langle |\delta| \rangle$ were estimated in the usual way as the empirical standard deviation in their measured values over the five realizations, divided by $\sqrt{5}$.

For comparison with the MC simulations, we solved the mean-field equation of motion for the single-step PDF, Eq. (13), numerically by a first-order iterative scheme with a time step of 10^{-4} MCSS (shorter time steps made no discernible difference). Both the simulations and the solution of the equation of motion were started from a sharp interface at $t=0$. Results for fields between 0 and $10J$ are shown in Fig. 3.

In general, we find overall qualitative agreement between the simulations and the equation of motion. For $T=0.2T_c$ and $|H| \leq 2J$, both methods have reached a common stationary value by $t=10\,000$ MCSS, while for $T=0.6T_c$ and $|H| \leq 3J$, stationarity is reached by $t=1\,000$ MCSS. Our choice of 5000 UPS as “warm-up time” in our studies of the stationary properties, corresponding to at least 10 000 MCSS, is thus well justified. However, there are significant quantitative differences between the simulation results and the solution of Eq. (13) for early times. We believe this indicates that the mean-field assumption of statistically independent step heights is not well justified until the interface structure has been randomized through a sufficient number of updates.

For the extremely strong field, $H=10J$, $\mathcal{W}(\delta \rightarrow \delta \pm 1) \approx \mathcal{W}(\delta \pm 1 \rightarrow \delta) \approx 1/2$ [see Eq. (14)], with equality in the limit $H/J \rightarrow \infty$. In this limit the evolution of the interface width is essentially diffusional and $\langle |\delta| \rangle \propto t^{1/2}$ without saturation at any finite time. Thus, the growth changes from the KPZ universality class for finite fields (with increasing saturation value of $\langle |\delta| \rangle$ as H increases), to the universality class of the random-deposition model [5], in which $\langle |\delta| \rangle$ grows without bound, for infinite field. As seen in Fig. 3(b), both methods agree with this result, although the amplitude for the MC simulation is larger than predicted by the mean-field equation of motion.

B. Stationary single-step probability densities

Stationary single-step PDFs were obtained by MC simulation at $T=0.2T_c$ and $0.6T_c$ for $\phi=0$ and several values of H between 0 and $3.0J$. The simulation results for $p[\delta]$ are

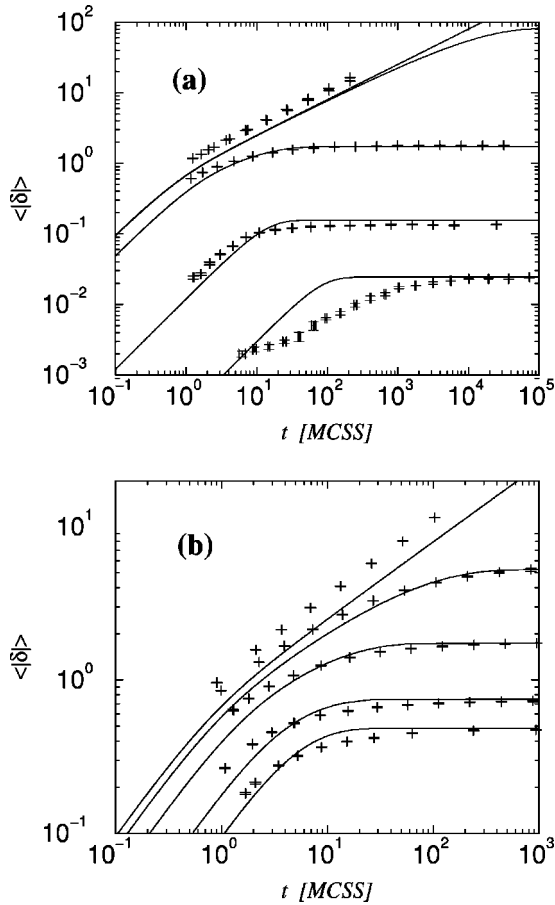


FIG. 3. Log-log plots of the mean step height $\langle |\delta| \rangle$ vs time t (in MCSS) as predicted by the mean-field equation of motion for the single-step PDF, Eq. (13) (solid curves), and by dynamic MC simulations (crossed error bars indicating statistical standard errors in t and $\langle |\delta| \rangle$). From bottom to top, the results shown are for $H/J = 0, 1, 2, 3$, and 10 [MC results for $H/J = 10$ in part (b) only]. (a) $T = 0.2T_c$. (b) $T = 0.6T_c$.

shown in Fig. 4, together with the theoretical result, Eq. (3) with $X(T, H)$ from Eq. (18). For both temperatures, the agreement is excellent in the whole range of δ and H shown.

A simple comparison between the analytical and simulation results is given in Fig. 5(a), which shows $\langle |\delta| \rangle$ vs H for $\phi = 0$ at $T = 0.2T_c$ and $0.6T_c$. The solid curves represent the theoretical result obtained by summation of Eq. (3), $\langle |\delta| \rangle = 2X/(1 - X^2)$, with X from Eq. (18). There is excellent agreement between the theoretical field dependence and the MC data. Additional confirmation of the form of the single-step PDF, Eq. (3), is obtained from the simulation results by calculating $\langle |\delta| \rangle$, both directly by summation over the numerically obtained PDF and from the probability of zero step height as $\langle |\delta| \rangle = \{p[0]^{-1} - p[0]\}/2$.

A slightly different way to check the agreement between the analytical predictions and the simulation results for the single-step PDF, is to compare $X(T, H)$ as given by Eq. (18) with the same quantity obtained from the simulations under the assumption that Eq. (3) holds. From this equation for the PDF, using $Z(0)$ from Eq. (6), it follows that X is given in terms of $p[0]$ as $X = \{1 - p[0]\}/\{1 + p[0]\}$, and in terms of

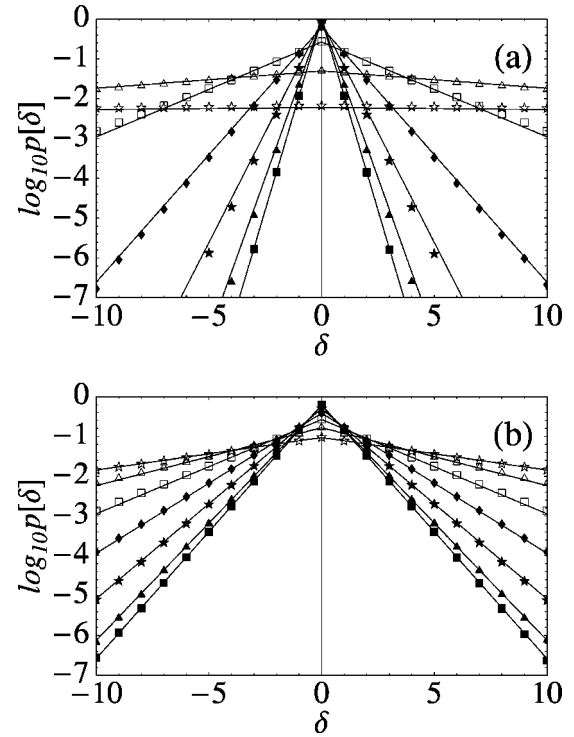


FIG. 4. MC (data points) and analytical (solid lines) results for the stationary single-step PDF, shown on logarithmic scale vs δ . The fields are $H/J = 0$ (filled squares), 0.5 (filled triangles), 1.0 (filled stars), 1.5 (filled diamonds), 2.0 (empty squares), 2.5 (empty triangles), and 3.0 (empty stars). (a) $T = 0.2T_c$. (b) $T = 0.6T_c$.

$\langle |\delta| \rangle$ as $X = \sqrt{1 + \langle |\delta| \rangle^{-2}} - \langle |\delta| \rangle^{-1}$. Both these MC estimates for $X(T, H)$ are shown in Fig. 5(b). Again, the agreement is excellent. The slight deviations of the estimate based on $\langle |\delta| \rangle$ for large H are probably due to the fact that data were only recorded in separate bins for $|\delta| < 64$, so that the calculated average becomes inaccurate whenever higher steps cannot be ignored. The estimate based on $p[0]$ does not suffer from this problem. However, the slight discrepancy between both MC estimates on the one hand and Eq. (18) on the other, which is seen between $H/J = 0.5$ and 2 for $T = 0.2T_c$, is probably a real effect.

C. Stationary interface velocities

In this section we compare the simulated interface velocities with the analytical approximation, Eq. (10). Figure 6 shows the normal velocity vs H for $\phi = 0$. Included are both the linear-response approximation (i.e., $X = e^{-2\beta J_x}$) and the nonlinear-response result with $X(T, H)$ from Eq. (18). Overall, there is excellent agreement between the MC results and the nonlinear-response theory, while the linear-response approximation seriously underestimates the velocity, especially at the lower temperature. As for the Ising model with hard Glauber dynamics studied in Ref. [7], these results show that the latter approximation is clearly inadequate, and we include no further linear-response results in this paper. (The apparent agreement between the linear-response approximation and the simulations for large H/J is simply a consequence of the fact that the normal velocity is bounded

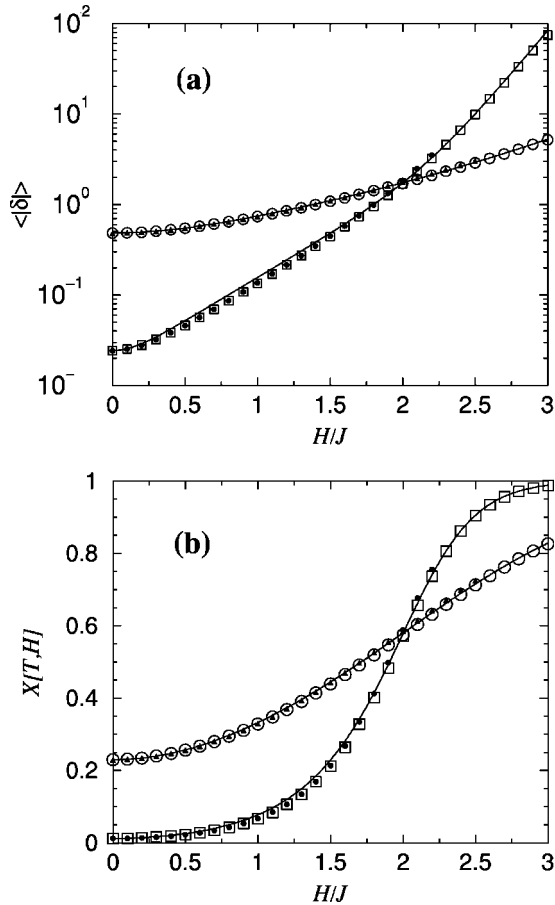


FIG. 5. (a) Average stationary step height $\langle |\delta| \rangle$, shown on logarithmic scale vs H for $\phi=0$ at $T=0.2T_c$ and $0.6T_c$. The curves represent the theoretical result. The MC data were obtained directly by summation over the simulated single-step PDFs (filled symbols) and from the probability of zero step height (empty symbols). See text for details. Curve with filled circles and empty squares, $T = 0.2T_c$. Curve with filled triangles and empty circles, $T = 0.6T_c$. (b) The stationary PDF width parameter $X(T, H)$ vs H , the analytical result Eq. (18) (curves) and estimates based on MC simulation results with $\phi=0$ for $p[0]$ (empty symbols) and for $\langle |\delta| \rangle$ (filled symbols). See text for details. Curves and symbols have the same interpretations as in (a). In this and all the following figures, the statistical uncertainty is much smaller than the symbol size.

by unity for the SOS model. This is *not* the case when SOS-violating transitions are allowed. In this case the linear-response approximation differs significantly from the nonlinear-response result and the simulations for strong fields, as shown in Fig. 2 of Ref. [7].) A slight disagreement between the simulations and the analytical predictions is seen at $0.2T_c$ in the same range of field values as for $X(T, H)$ obtained from the single-step PDF in Sec. IV B.

The dependence of the normal velocity on the tilt angle ϕ is shown in Fig. 7 for several values of H/J between 0.1 and 3.0. At $T=0.2T_c$ the anisotropy undergoes a gradual change from increasing with ϕ in agreement with the polynuclear growth model at small angles and the single-step model for larger angles at weak fields, to Eden-type inverse anisotropy [33–35] at strong fields [Fig. 7(a)]. At $T=0.6T_c$, on the

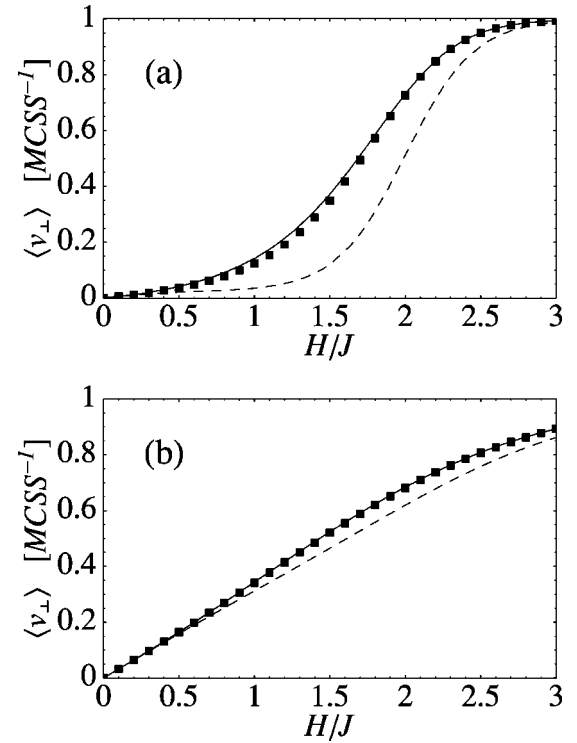


FIG. 6. The average stationary normal interface velocity $\langle v_{\perp} \rangle$ vs H for $\phi=0$. The MC results are shown as data points, the linear-response results as dashed curves, and the nonlinear-response results as solid curves. (a) $T=0.2T_c$. (b) $T=0.6T_c$.

other hand, inverse anisotropy is found for the stronger fields, growing gradually more pronounced with increasing H [Fig. 7(b)], while for the weakest fields studied the velocity is nonmonotonic in $\tan \phi$ [Fig. 7(c)]. The agreement between the simulations and the analytical results is excellent everywhere.

The temperature dependence of the normal interface velocity is shown in Fig. 8 for several values of H/J between 0.2 and 3.0. The agreement between the simulations and the analytical results is excellent everywhere. This figure shows clearly that as T is lowered, the velocity changes increasingly steeply from zero to unity at $H/J=2$, developing a step discontinuity at $T=0$. This result could also have been suspected by comparing Figs. 6(a) and 6(b).

D. Spin-class populations and skewness

A closer look at the performance of the mean-field approximation for the interface structure is provided by the mean spin-class populations. The analytical predictions for the class populations are based on the assumption that different steps are statistically independent. A comparison of the simulation results with the analytical predictions therefore gives a way of testing this assumption.

The six mean class populations, $\langle n(01s) \rangle$, $\langle n(11s) \rangle$, and $\langle n(21s) \rangle$ with $s = \pm 1$ are shown vs H in Fig. 9 for $\phi=0$ and $T=0.2T_c$ and $0.6T_c$. At both temperatures the analytical approximations follow the average of the populations for $s = +1$ and $s = -1$ quite well, but at intermediate fields in particular, the populations in front of the surface ($s = -1$) and

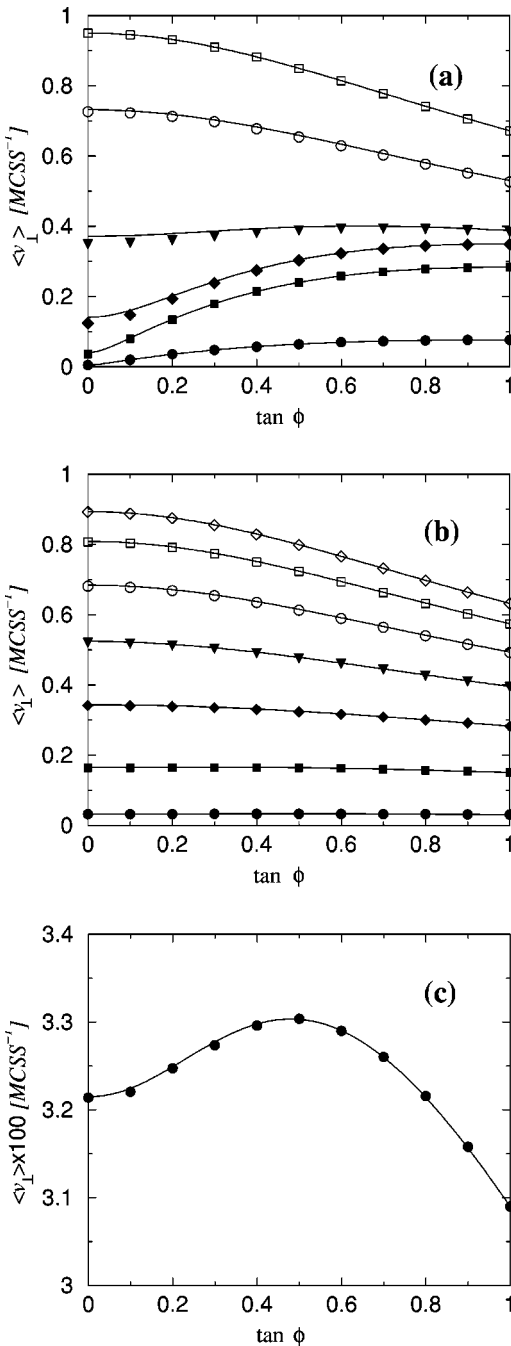


FIG. 7. The average stationary normal interface velocity $\langle v_{\perp} \rangle$ vs $\tan \phi$ for several values of H . MC data are represented by data points, and analytical results by solid curves. (a) $T = 0.2T_c$. (b) $T = 0.6T_c$. In parts (a) and (b), the values of H/J are (from below to above), 0.1, 0.5, 1.0, 1.5, 2.0, 2.5, and 3.0 [in (b) only]. (c) $H/J = 0.1$ for $T = 0.6T_c$, shown on a magnified scale to reveal the non-monotonic dependence on $\tan \phi$ for this very weak field.

behind it ($s = +1$) are distinctly different.

The skewness between the spin populations on the leading and trailing edges of the interface are a consequence of short-range correlations between neighboring steps, and it is quite commonly observed in driven interfaces. This is the case, even when the *long-range* correlations vanish as they do for interfaces in the KPZ dynamic universality class, to which

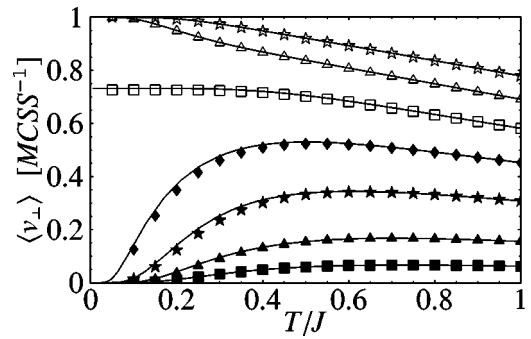


FIG. 8. The average stationary normal interface velocity $\langle v_{\perp} \rangle$ vs T for $\phi = 0$. MC data are represented by data points, and analytical results by solid curves. From below to above, the values of H/J are 0.2, 0.5, 1.0, 1.5, 2.0, 2.5, and 3.0.

the present model belongs for all finite, nonzero values of H . Such skewness was also observed in our study of the Ising model in Ref. [7], but in that case it was difficult to separate it from the effects of bubbles and overhangs. Skewness has also been observed in several other SOS-type models, such as the body-centered SOS model studied by Neergaard and den Nijs [18], the model for step propagation on crystal surfaces with a kink-Ehrlich-Schwobel barrier studied by Pierre-Louis *et al.* [19], and a model for the local time horizon in parallel MC simulations studied by Korniss *et al.* [20]. (However, no skewness is observed for the soft Glauber dynamic, a result which may be general for soft dynamics.) The correlations associated with the skewness generally lead to a broadening of protrusions on the leading edge (“hilltops”),

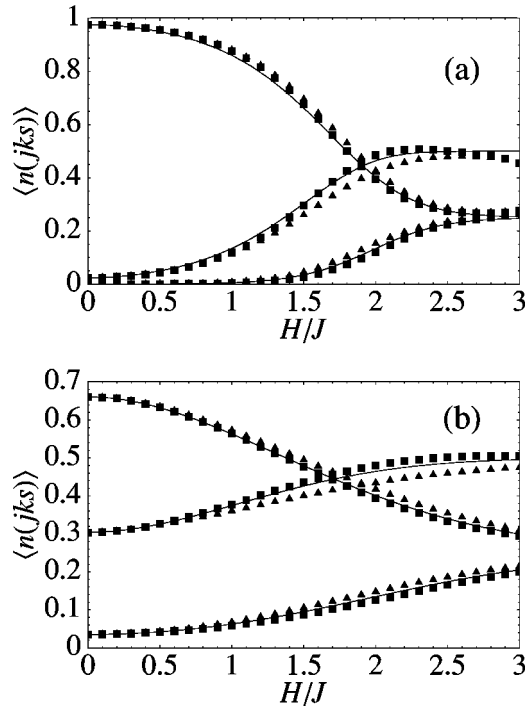


FIG. 9. Mean stationary class populations $\langle n(jks) \rangle$ vs H for $\phi = 0$. (a) $T = 0.2T_c$. (b) $T = 0.6T_c$. From top to bottom at the left edge of both parts, the classes are 01s, 11s, and 21s with squares representing MC data for $s = +1$ and triangles for $s = -1$. The analytical approximations are indicated by the solid curves. Note the different vertical scales in the two parts.

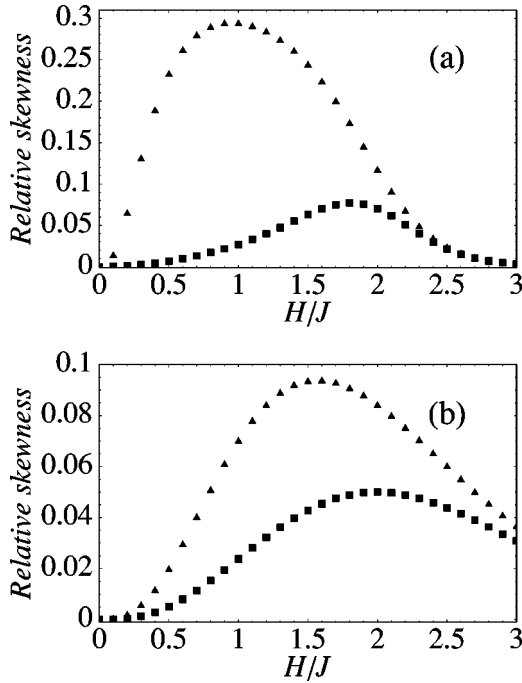


FIG. 10. The two relative skewness parameters ρ (triangles) and ϵ (squares), defined in Eqs. (20) and (21), respectively. The parameters are shown vs H for $\phi=0$. (a) $T=0.2T_c$. (b) $T=0.6T_c$. Note the different vertical scales in the two parts.

while those on the trailing edge (“valley bottoms”) are sharpened [18], or the other way around [20]. In terms of spin-class populations, the former corresponds to $\langle n(21-) \rangle > \langle n(21+) \rangle$ and $\langle n(11+) \rangle > \langle n(11-) \rangle$. The relative skewness can therefore be quantified by the two functions,

$$\rho = \frac{\langle n(21-) \rangle - \langle n(21+) \rangle}{\langle n(21-) \rangle + \langle n(21+) \rangle}, \quad (20)$$

introduced in Ref. [18], and

$$\epsilon = \frac{\langle n(11+) \rangle - \langle n(11-) \rangle}{\langle n(11+) \rangle + \langle n(11-) \rangle}. \quad (21)$$

These two skewness parameters are shown together in Fig. 10. The relative skewness is seen to be considerably stronger at the lower temperature. This temperature dependence is especially pronounced for ρ .

Yet another way to visualize the skewness is to consider the joint two-step PDF, $p[\delta(x), \delta(x+1)]$. Logarithmic contour plots of this quantity for different values of H are shown in Fig. 11 for $\phi=0$ at $T=0.6T_c$. It is clearly seen how the contours change with H . For $H=0$ a symmetric diamond shape with equidistant contours indicates statistical independence with single-step PDFs given by Eq. (3). For stronger fields we find shapes that are elongated in the second quadrant [$\delta(x) < 0, \delta(x+1) > 0$] and foreshortened in the fourth quadrant [$\delta(x) > 0, \delta(x+1) < 0$]. This shape indicates that large negative $\delta(x)$ tend to be followed by large positive $\delta(x+1)$ (sharp valleys), while positive $\delta(x)$ tend to be followed by smaller negative $\delta(x+1)$ (rounded hilltops).

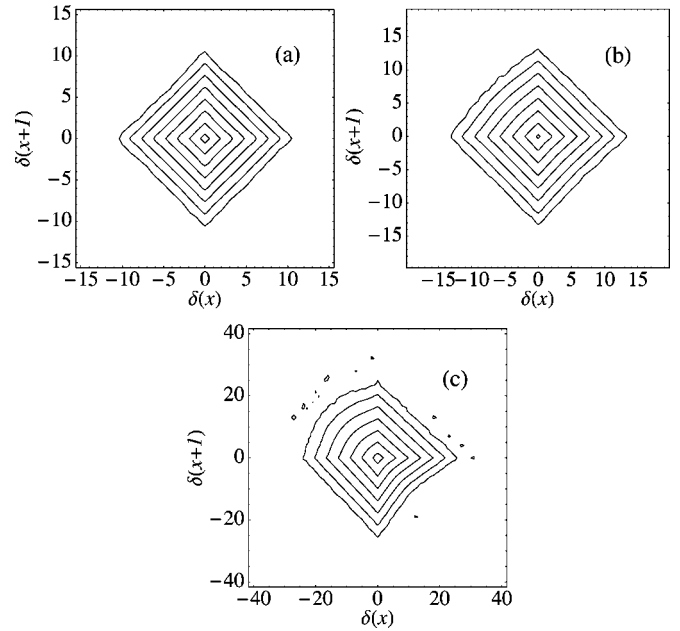


FIG. 11. Contour plots of $\log_{10} p[\delta(x), \delta(x+1)]$ for $\phi=0$ at $T=0.6T_c$. (a) $H/J=0$. (b) $H/J=1.0$. (c) $H/J=2.0$. Note the different scales in the three parts. See discussion in the text.

While the contour plots for interfaces with $\phi=0$ are always symmetric about the line $\delta(x+1) = -\delta(x)$, as seen in Fig. 11, for $\phi > 0$ corresponding to $\langle \delta \rangle > 0$, most of the probability is concentrated in the first quadrant [$\delta(x) > 0, \delta(x+1) > 0$], as shown for $\phi=45^\circ$ at $T=0.6T_c$ in Fig. 12. In the case of tilted interfaces, too, the symmetry about the line $\delta(x+1) = \delta(x)$, which is obeyed for $H=0$ [Fig. 12(a)], is gradually destroyed with increasing field [Fig. 12(b) and 12(c)]. We have not been successful in attempts to construct

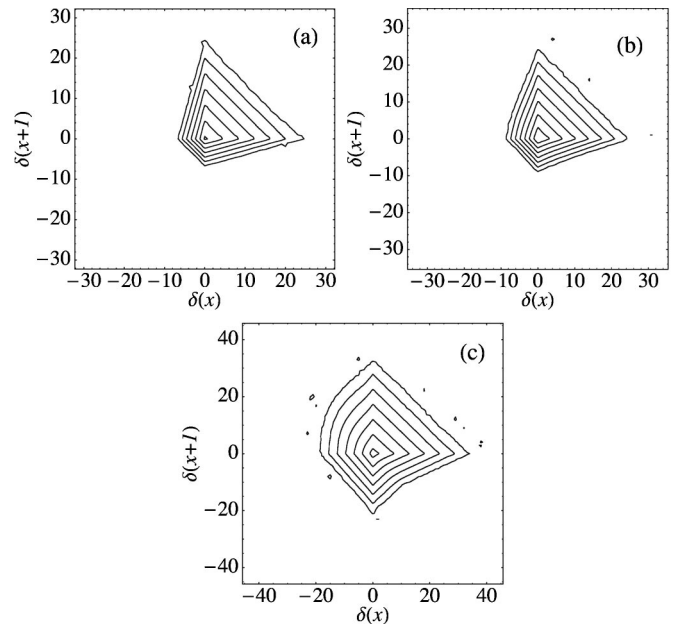


FIG. 12. Contour plots of $\log_{10} p[\delta(x), \delta(x+1)]$ for $\phi=45^\circ$ at $T=0.6T_c$. (a) $H/J=0$. (b) $H/J=1.0$. (c) $H/J=2.0$. Note the different scales in the three parts. See discussion in the text.

an analytical approximation which describes this evolution of the joint two-step PDF with increasing field.

V. CONCLUSION

In this paper, we have considered in detail the microstructure of an unrestricted solid-on-solid (SOS) interface with Glauber dynamics, which is driven far from equilibrium by an applied field. The microstructure is of interest because it determines a number of interface properties, such as mobility and chemical reactivity. We adapted to this model a mean-field, nonlinear-response approximation previously developed for driven Ising interfaces without the SOS restriction [7]. In comparison to the Ising driven interface, which leaves bubbles of the unstable phase in its wake and exhibits “overhangs,” the SOS interface is a relatively simple object. The absence of overhangs and of fluctuations in the stable and unstable phases (bubbles behind and in front of the interface) makes the SOS interface more suitable for description in terms of a mean-field type model. Moreover, unlike the Ising model, in which there are several effects that simultaneously contribute to the inaccuracy of the approximate treatment, the simpler SOS structure makes it possible to identify the short-range correlations as the only significant factor causing deviations between the true interface behavior and the mean-field theory.

To study the microstructure of the interface in detail, we investigated the interface velocity as a function of driving field, temperature, and angle relative to the lattice axes. We also studied the local shape of the interface in terms of the spin-class populations and the probability density for individual steps in the interface. In essentially all cases we found excellent agreement between our theoretical description of the stationary moving interface and the results of our dynamic MC simulations.

The microstructure of the moving interface depends crucially on the details of the stochastic dynamics, and for the Glauber dynamic used here, the average height of a step in the interface was found to increase strongly with the applied field. Our theory predicts that this should be the case (with quantitative variations depending on the particular dynamic) for any dynamic in which the single-spin transition rates cannot be factorized into a part that depends only on interaction energies and another that depends only on the applied field (hard dynamics [16]). In contrast, for factorizing (soft) dynamics the interface structure should remain independent of the field. This was recently confirmed for the unrestricted SOS interface by MC simulations [15]. It is therefore important to use great caution in drawing conclusions about the microstructure of driven interfaces, based on dynamic MC

simulations. For such conclusions to be valid, the dynamic must be chosen appropriately to the physical system of interest. The hard type of dynamics would appear to be particularly suited for certain interfaces in magnetic or dielectric systems, where the local order parameter is not conserved. The dynamics of such interfaces have in the past often been studied with standard Glauber or Metropolis dynamics. Soft dynamics would seem more appropriate for solidification or adsorption problems where the driving force is a chemical-potential difference [36,37], although diffusion often plays a complicating role in these cases.

To avoid any misunderstandings, we emphasize that the soft/hard classification refers to the *dynamic*, and *not* to the Hamiltonian. As discussed both in this paper and in Ref. [15], a system described by a particular Hamiltonian could evolve according to a hard or a soft dynamic, depending on the physical characteristics of the transition processes. A more thorough discussion of the physical aspects of the differences between hard and soft dynamics will be included in a forthcoming paper [38].

One aspect of the interface dynamics not completely captured by our model is, of course, the short-range correlations. Namely, within the mean-field approximation used here, individual steps of the interface are assumed to be statistically independent. However, for increasing fields the interface undergoes a gradual breakdown of up/down symmetry. This is clearly seen in our simulations here, as well as in several other examples of driven interfaces [7,18–20]. It would seem likely that one could construct a mean-field approximation at the two-step level, which might be able to predict this skewness for hard dynamics, as well as its absence for soft dynamics. However, such a theory has not yet been developed.

Finally we note that, by comparison with the theoretical and numerical results presented here and in Refs. [7] and [15], experimental observations of the driving-force dependence of interface step heights and their correlations for steady-state moving interfaces could add to our understanding of the underlying dynamic processes.

ACKNOWLEDGMENTS

We acknowledge useful conversations with B. Schmittmann and K. Kawasaki. P.A.R. appreciates the hospitality of the Faculty of Integrated Human Studies at Kyoto University. The research was supported in part by National Science Foundation through Grant Nos. DMR-9981815 and DMR-0120310, and by Florida State University through the Center for Materials Research and Technology and the School of Computational Science and Information Technology.

-
- [1] M.I. Mendelev and D.J. Srolovitz, *Acta Mater.* **48**, 3711 (2000); *ibid.* **49**, 589 (2001); *ibid.* **49**, 2843 (2001).
 [2] P.A. Rikvold, G. Brown, S.J. Mitchell, and M.A. Novotny, in *Nanostructured Magnetic Materials and their Applications*, edited by D. Shi, B. Aktas, L. Pust, and F. Mikailov, Springer

Lecture Notes in Physics, Vol. 593 (Springer, Berlin, 2002), p. 164.

- [3] S.V. Khare and T.L. Einstein, *Phys. Rev. B* **57**, 4782 (1998), and references therein.
 [4] L. da Silveira Lobo Sternberg, *Global Ecol. Biogeogr.* **10**, 369

- (2001).
- [5] A.-L. Barabási and H.E. Stanley, *Fractal Concepts in Surface Growth* (Cambridge University Press, Cambridge, 1995), and references therein.
- [6] P. Meakin, *Fractals, Scaling, and Growth far from Equilibrium* (Cambridge University Press, Cambridge, 1998), and references therein.
- [7] P.A. Rikvold and M. Kolesik, *J. Stat. Phys.* **100**, 377 (2000).
- [8] K. Kawasaki, in *Phase Transitions and Critical Phenomena*, edited by C. Domb and M. Green, (Academic, London, 1972), Vol. 2.
- [9] D.P. Landau and K. Binder, *Monte Carlo Simulations in Statistical Physics* (Cambridge University Press, Cambridge, 2000).
- [10] P. Devillard and H. Spohn, *Europhys. Lett.* **17**, 113 (1992).
- [11] H. Spohn, *J. Stat. Phys.* **71**, 1081 (1993).
- [12] R.A. Ramos, P.A. Rikvold, and M.A. Novotny, *Phys. Rev. B* **59**, 9053 (1999), and references therein.
- [13] M.A. Novotny, P.A. Rikvold, M. Kolesik, D.M. Townsley, and R.A. Ramos, *J. Non-Cryst. Solids*, **274**, 356 (2000).
- [14] W.K. Burton, N. Cabrera, and F.C. Frank, *Philos. Trans. R. Soc. London, Ser. A* **243**, 299 (1951).
- [15] P.A. Rikvold and M. Kolesik, *J. Phys. A* **35**, L117 (2002).
- [16] J. Marro and R. Dickman, *Nonequilibrium Phase Transitions in Lattice Models* (Cambridge University Press, Cambridge, 1999), Chap. 7.
- [17] M. Kardar, G. Parisi, and Y.-C. Zhang, *Phys. Rev. Lett.* **56**, 889 (1986).
- [18] J. Neergaard and M. den Nijs, *J. Phys. A* **30**, 1935 (1997).
- [19] O. Pierre-Louis, M.R. D’Orsogna, and T.L. Einstein, *Phys. Rev. Lett.* **82**, 3661 (1999).
- [20] G. Korniss, Z. Toroczkai, M.A. Novotny, and P.A. Rikvold, *Phys. Rev. Lett.* **84**, 1351 (2000).
- [21] C.N. Yang and T.D. Lee, *Phys. Rev.* **87**, 404 (1952); **87**, 410 (1952). The term “lattice gas” was apparently first used and its equivalence to the Ising model first discussed in these two papers [22].
- [22] R.K. Pathria, *Statistical Mechanics*, 2nd ed. (Butterworth-Heinemann, Oxford, 1996).
- [23] H.C. Kang and W.H. Weinberg, *J. Chem. Phys.* **90**, 2824 (1989); K.A. Fichthorn and W.H. Weinberg, *ibid.* **95**, 1090 (1989).
- [24] T. Ala-Nissila, J. Kjoll, and S.C. Ying, *Phys. Rev. B* **46**, 846 (1992).
- [25] A.B. Bortz, M.H. Kalos, and J.L. Lebowitz, *J. Comput. Phys.* **17**, 10 (1975).
- [26] M.A. Novotny, *Comput. Phys.* **9**, 46 (1995).
- [27] P. Meakin, P. Ramanlal, L.M. Sander, and R.C. Ball, *Phys. Rev. A* **34**, 5091 (1986).
- [28] M. Plischke, Z. Rácz, and D. Liu, *Phys. Rev. B* **35**, 3485 (1987).
- [29] J. Krug and H. Spohn, *Europhys. Lett.* **8**, 219 (1989).
- [30] J. Kertész and D.E. Wolf, *Phys. Rev. Lett.* **62**, 2571 (1989).
- [31] L. Onsager, *Phys. Rev.* **65**, 117 (1944).
- [32] While $L_x=1000$ would give adequate accuracy for velocities and class populations, the PDFs (especially the two-step ones) required $L_x=10\,000$ to yield acceptable results. Interestingly, simulations for $L_x=10\,000$ took only about twice as long as for $L_x=1000$. We attribute this to the changing cache-friendliness of our highly dynamic simulation code. Each simulation run for a specific set of values of all parameters took approximately 9 h on a DEC Alpha Unix workstation, 4 h on a Pentium II PC running LINUX, or 1 h on an AMD Athlon PC running LINUX.
- [33] D. Dhar, in *On Growth and Form: Fractal and Non-Fractal Patterns in Physics*, edited by H.E. Stanley and N. Ostrowsky (Martinus Nijhoff, Dordrecht, 1986), p. 288.
- [34] P. Meakin, R. Jullien, and R. Botet, *Europhys. Lett.* **1**, 609 (1986).
- [35] R. Hirsch and D.E. Wolf, *J. Phys. A* **19**, L251 (1986).
- [36] H. Guo, B. Grossmann, and M. Grant, *Phys. Rev. Lett.* **64**, 1262 (1990).
- [37] M. Kotrla and A.C. Levi, *J. Stat. Phys.* **64**, 579 (1991).
- [38] P.A. Rikvold and M. Kolesik (unpublished).